Supplementary Figures

A

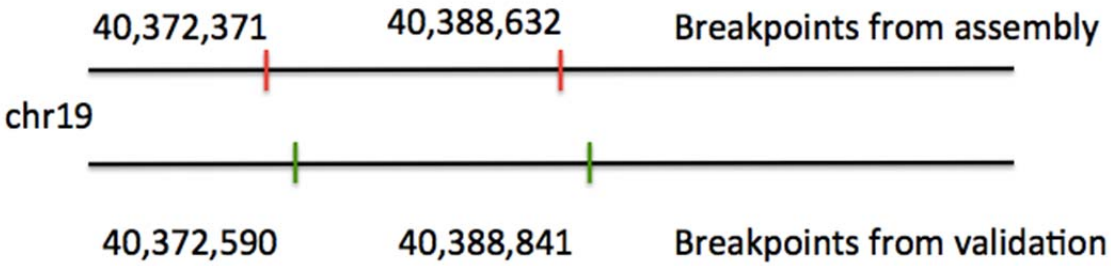

B

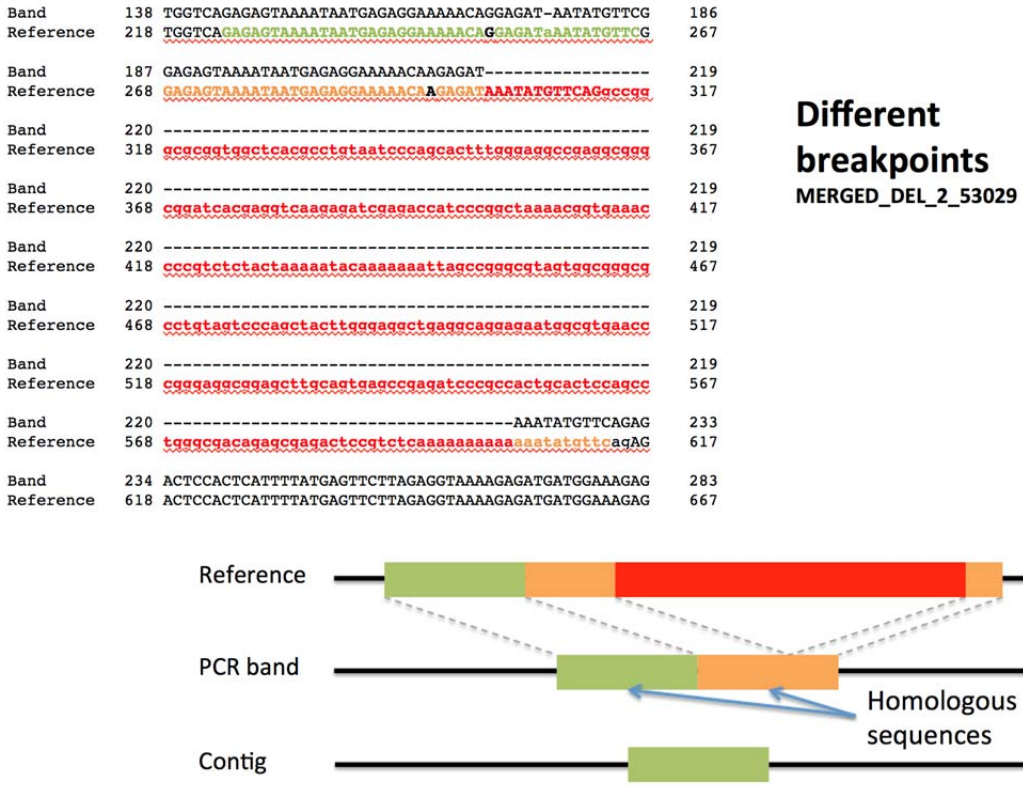

Supplementary Figure 1. Examples of discrepancies in predicted and validated breakpoint coordinates. A) Most frequently, predicted breakpoints were shifted relative to those derived from validation excesses. One such example is depicted. All such cases were removed by post validation filters. B) In one case (chr9:35803108-35803461) assembly collapsed tandem repeat around breakpoints resulting in shorter contig and overestimated breakpoints.

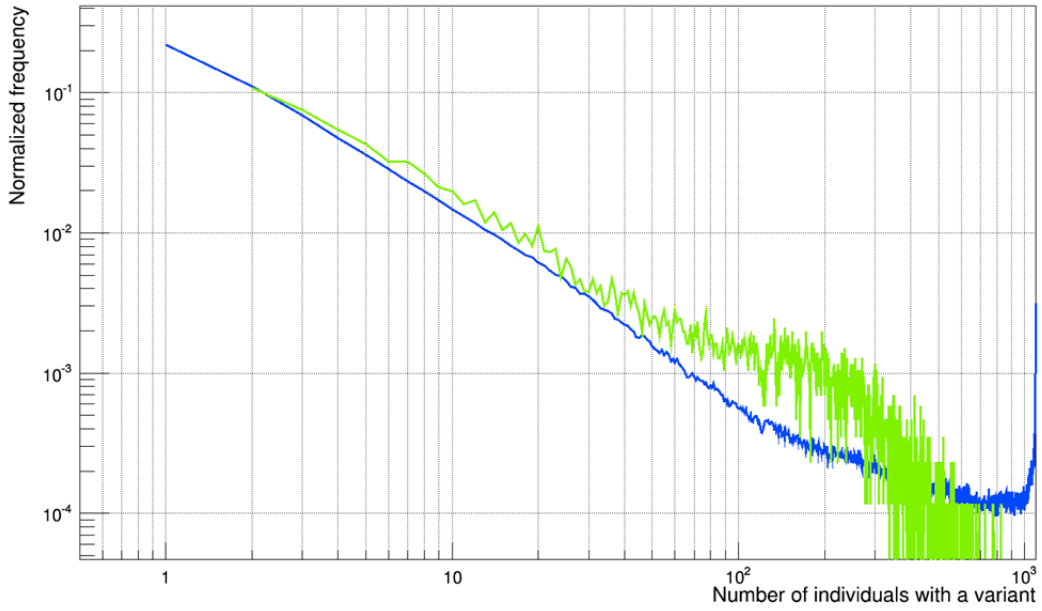

A

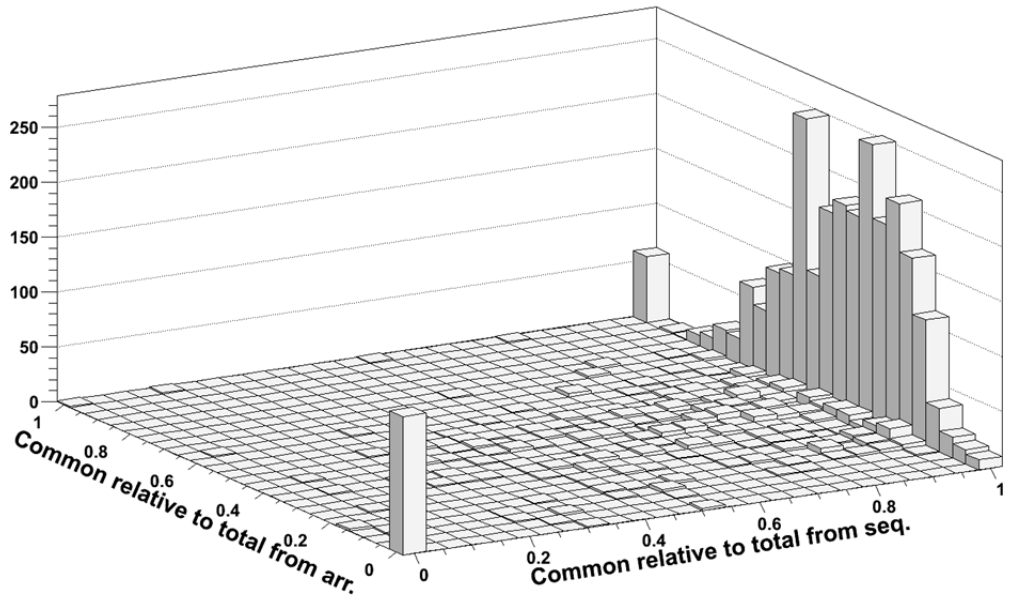

B

Supplementary Figure 2. Variant sample frequency spectrum. A) Frequency for bi-allelic SNPs[1] is in blue, while frequency for deletions in the this study is in green. SNPs and deletions were discovered from the same 1,092 individuals. B) Correlation of samples genotyped as having deletion from OMNI SNP genotyping array (y-axis) and from mapping reads to sequences of breakpoint junctions (x-axis) in 292 samples. Values on x/y axis is the fraction of samples with deletion common between the two ways of genotyping divided by the number of samples genotypes as having deletion by read mapping/by OMNI SNP array. Number of deletions with such fractions is on z-axis. Genotyping from sequencing, i.e., from mapping reads to sequence of deletion junctions, underestimates frequency of deletion by roughly 60%. Therefore, the true frequency spectrum for deletion in A, is shifter right.

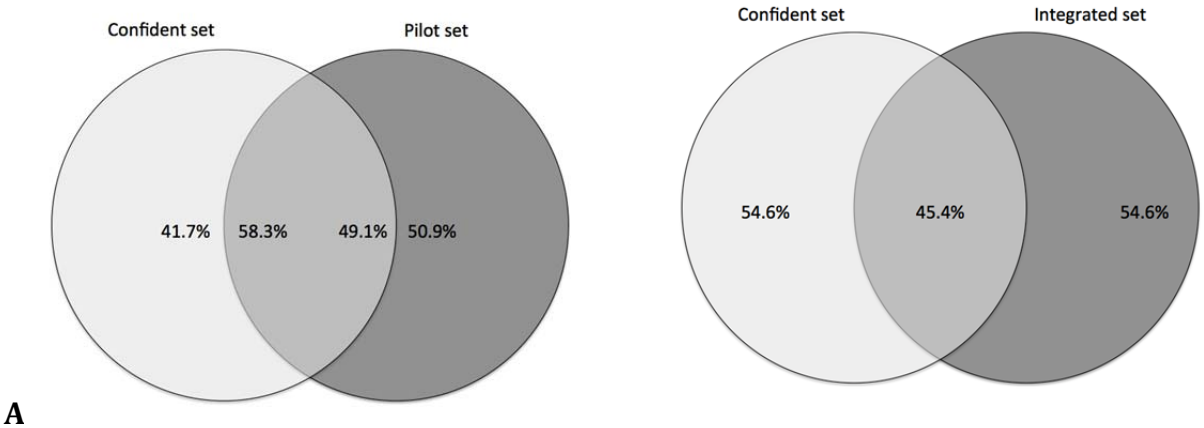

A

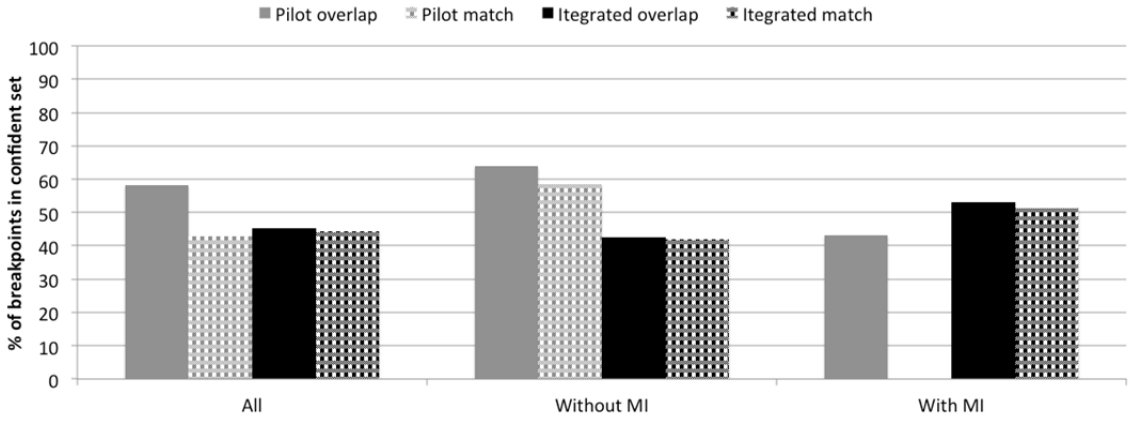

B

Supplementary Figure 3. Comparison of confident set of breakpoints with pilot and integrated sets of breakpoints. A) Fraction of SV breakpoints that overlap 50% reciprocally between sets. B) Breakdown of confident breakpoints with/without MIs by 50% reciprocal overlap and exact match to breakpoints in pilot/integrated sets. For exact match we only matched start and end of the breakpoints. Overlap is higher with pilot set, but there is marked difference in the fraction of overlapping and exactly matching breakpoints to pilot set. The difference is particularly drastic for breakpoints with MIs, demonstrating that pilot set was particularly limited in resolving MIs. The difference is minor when comparing to integrated set. However, integrated set represented deletion breakpoint in a narrow size range (**Fig. 1C**).

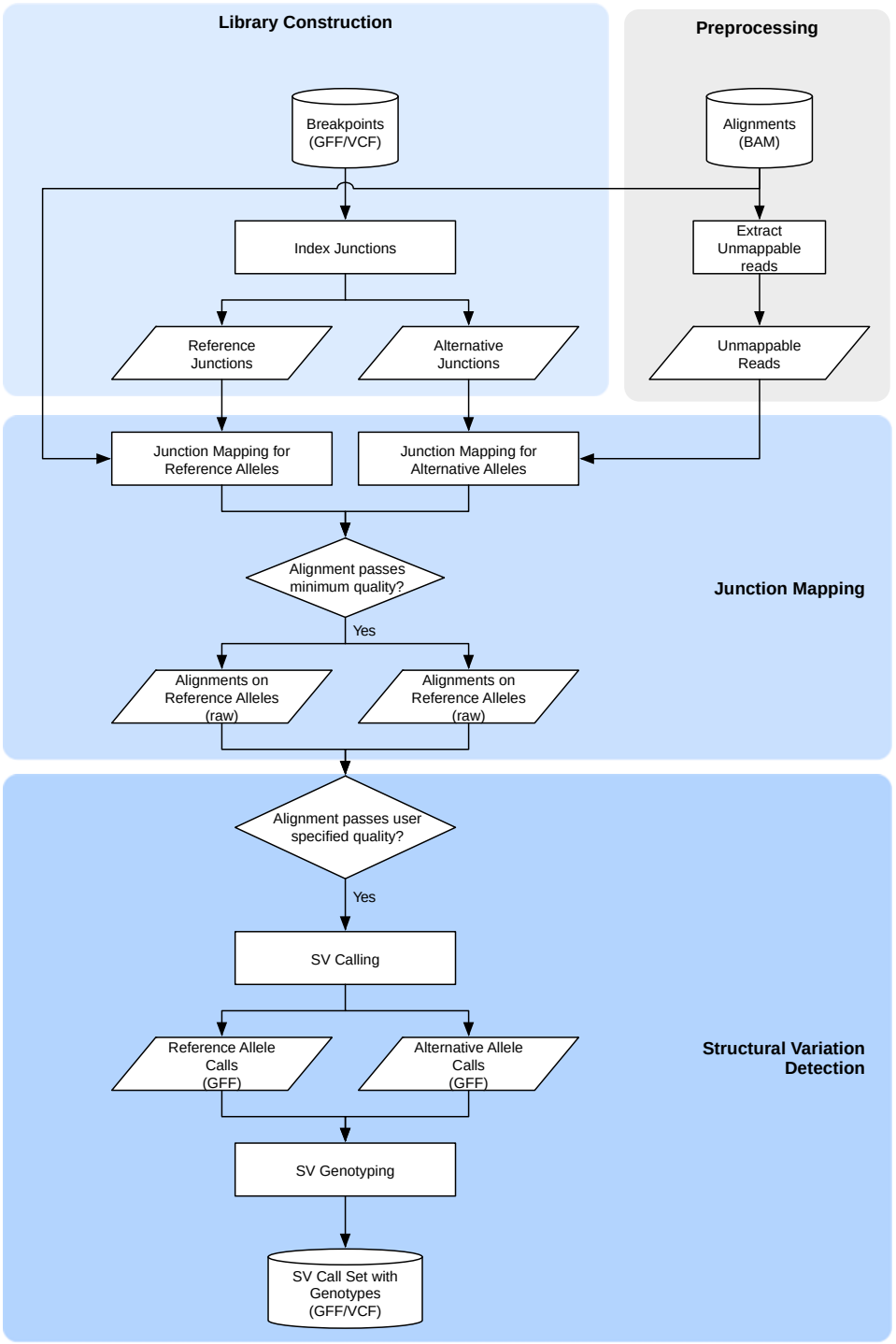

Supplementary Figure 4. BreakSeq2 workflow. Reads which are unmapped, soft-clipped or badly mapped are considered unmappable against the reference genome. Further filtering based on the mapping quality and the edit distances of the alignment against the reference genome is done to narrow down the list of unmappable reads. Alignments of the unmappable reads against the breakpoint library is used to gather evidence for SVs. The more comprehensive the breakpoint library is, the better BreakSeq2 is expected to perform.

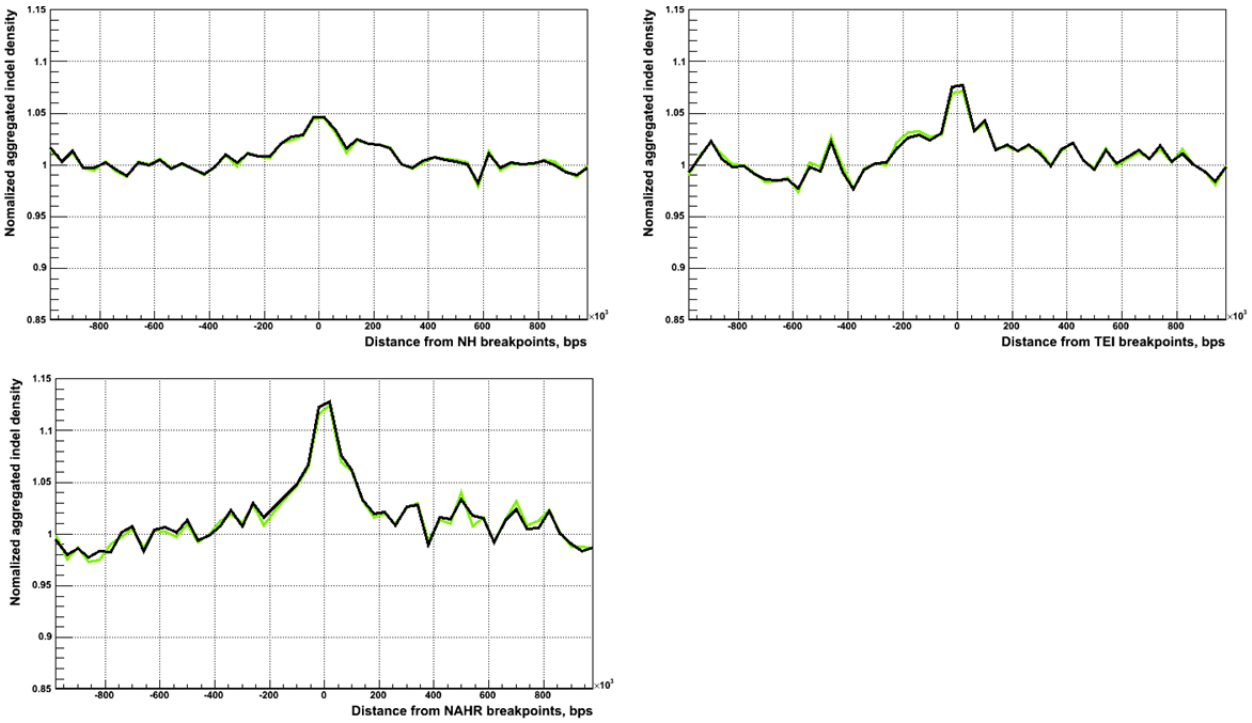

Supplementary Figure 5. Indel aggregation around deletion breakpoints. Aggregation for indels of 1-6 bps in length is in black; aggregation for indels of 1 bp in length is in green.

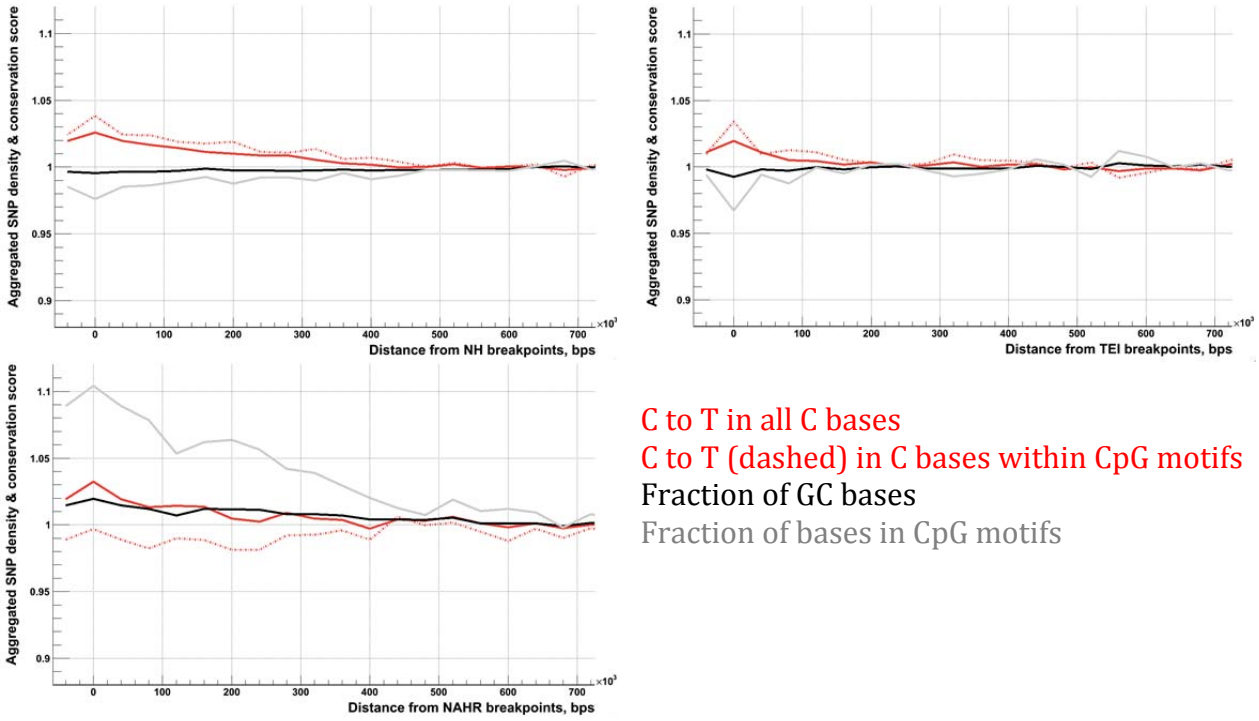

Supplementary Figure 6. C to T mutations, GC content and CpG contents around breakpoints of different classes. All curves are normalized to unity at tails. Only unmasked bases, i.e. those where the 1000 Genomes Project can do confident SNP calling, were used in the analysis. NAHR breakpoints show very different distributions from the breakpoints of other classes. They do show increase in GC and CpG content while NH and TEI do not. Frequency of C to T substitutions also decreases in CpG motifs around NAHR while increases around NH and TEI. The latter may imply association of NAHR with regions of lower methylation and association of NH and TEI with regions of higher methylation.

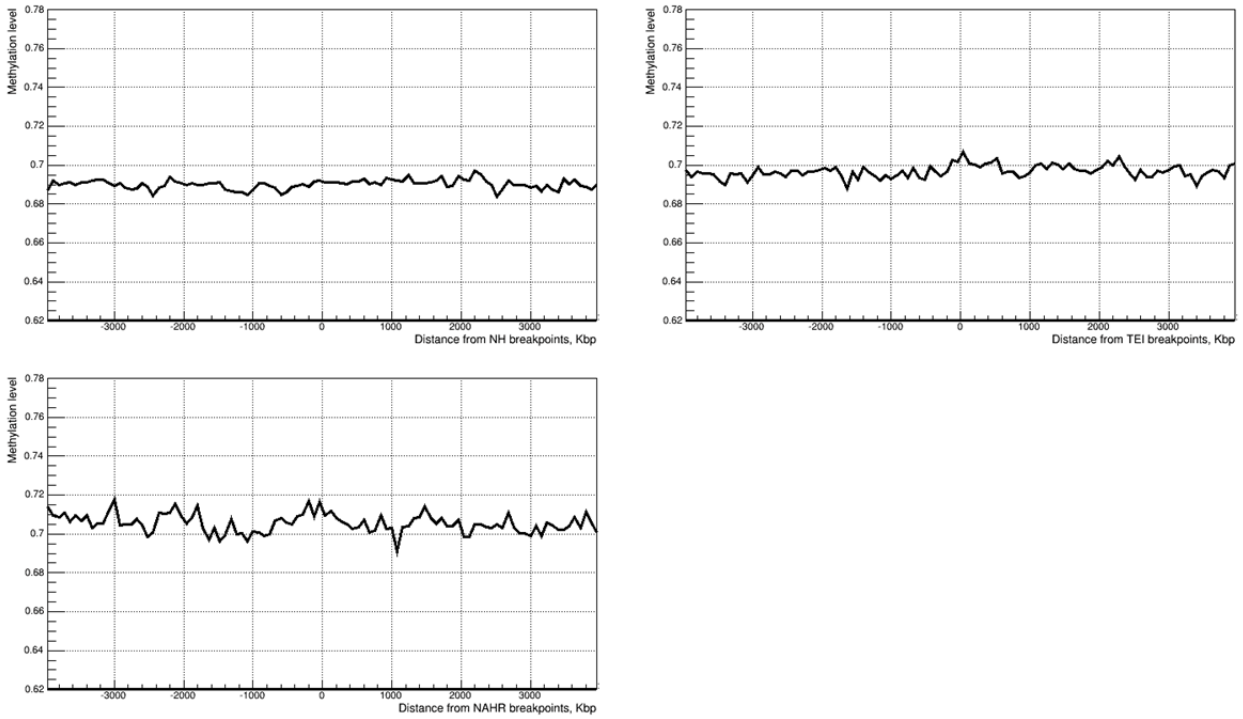

Supplementary Figure 7. Methylation levels in H1ESC cell line around breakpoints of different classes. There is no noticeable change in methylation level around breakpoints of either class. On a smaller scale we do observed increase in methylation level in the regions of about 1 kbp around breakpoints of each type (data not shown). Though, this could be technical artifact, as breakpoints generally have higher repeat content and all calculated values, including methylation level, will be prone to mistakes in such regions. For instance, SNPs densities in unmasked sites showed sharp increase in such proximity to breakpoints.

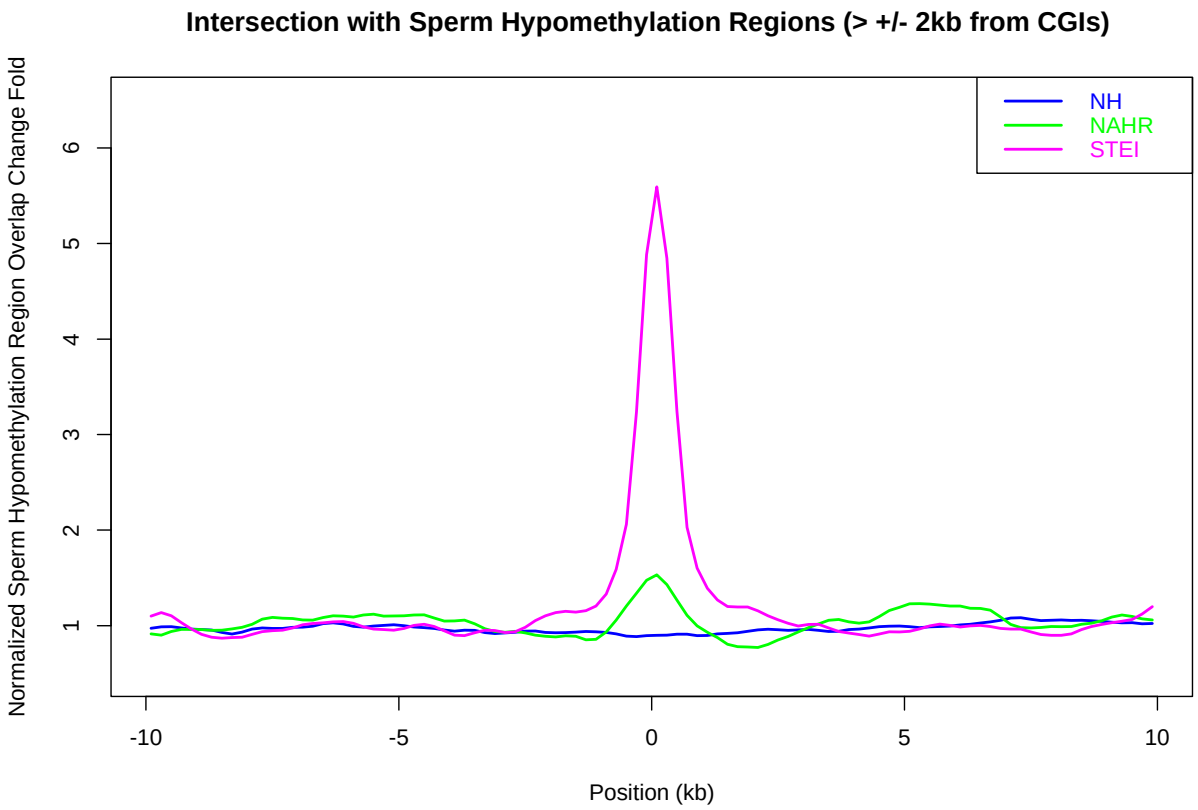

Supplementary Figure 8. Overlap of breakpoints with hypomethylated regions in sperm. Only regions outside of 2 kbp windows of CpG islands were considered. Coordinates of CpG islands were downloaded from the following web-address[2]
http://epigraph.mpi-inf.mpg.de/download/CpG_islands_revisited

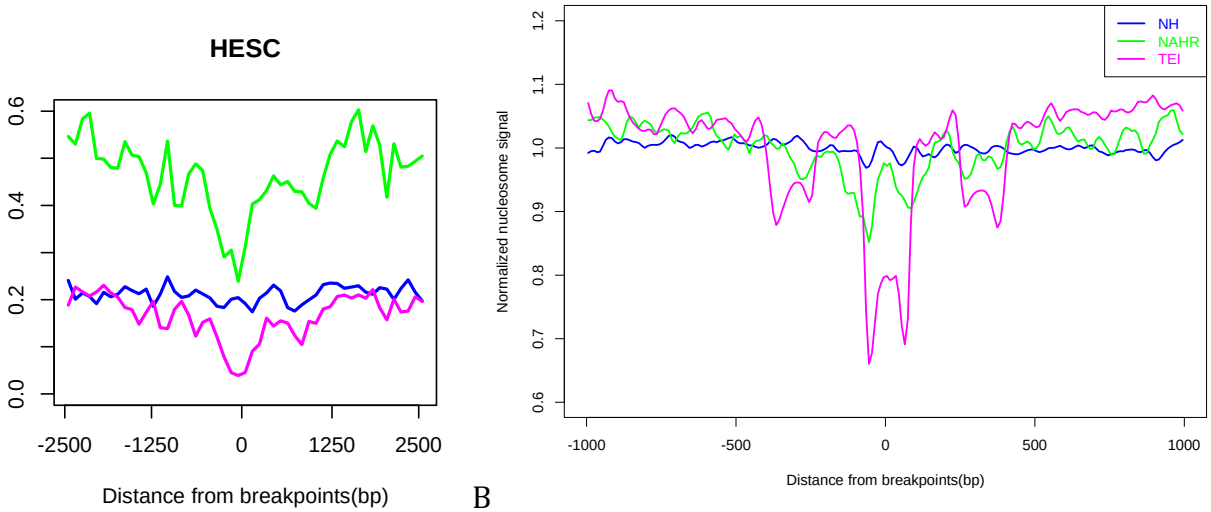

A B

Supplementary Figure 9. A) Aggregation of DNase peaks (in hESC cells) around breakpoints of different classes. NAHR breakpoints have overall higher DNase signal, suggesting association with accessible/functional DNA, consistent with association with open chromatin. However, exact NAHR breakpoint locations avoid accessible/functional chromatin (dip in the curve), which could be the result of negative selection. B) Aggregation of nucleosome occupancy in NA12878 cell line. TEI breakpoints are strongly associated with nucleosome free DNA. NAHR breakpoints exhibit weak association, while NH breakpoints have no association.

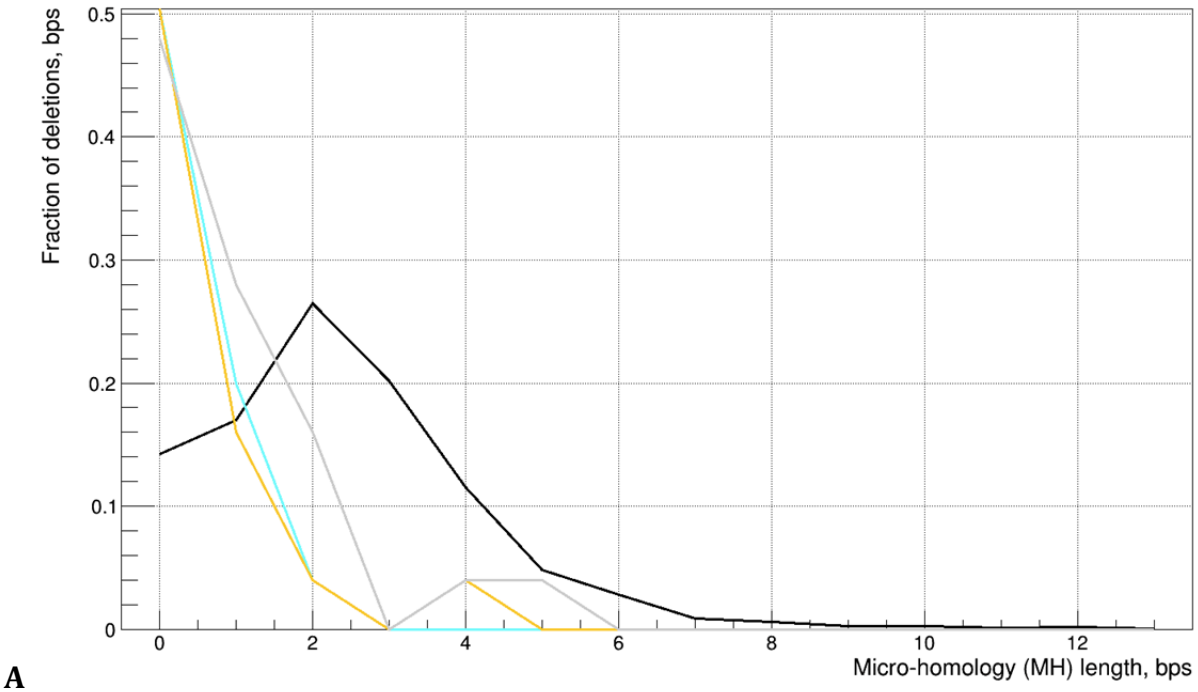

A

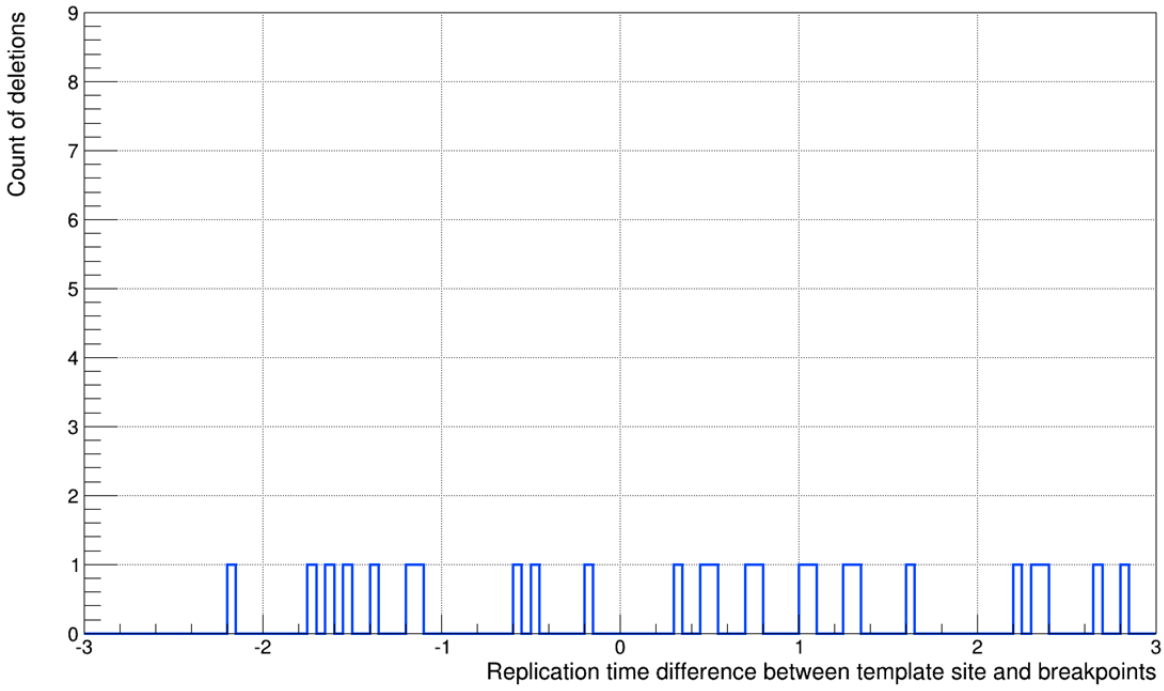

B

Supplementary Figure 10. Analysis of micro-insertions (MI) with template sites on different chromosome from the deletion. A) Length of micro-homology (MH) at deletion junction is not different from random (see also **Fig. 4**). For deletions with MIs and identified template site, MHs are calculated for 5'-ends/3'-ends of the deletion and the template site. B) The difference in replication time between template site and breakpoints does not reveal significant later or earlier replication time of template sites.

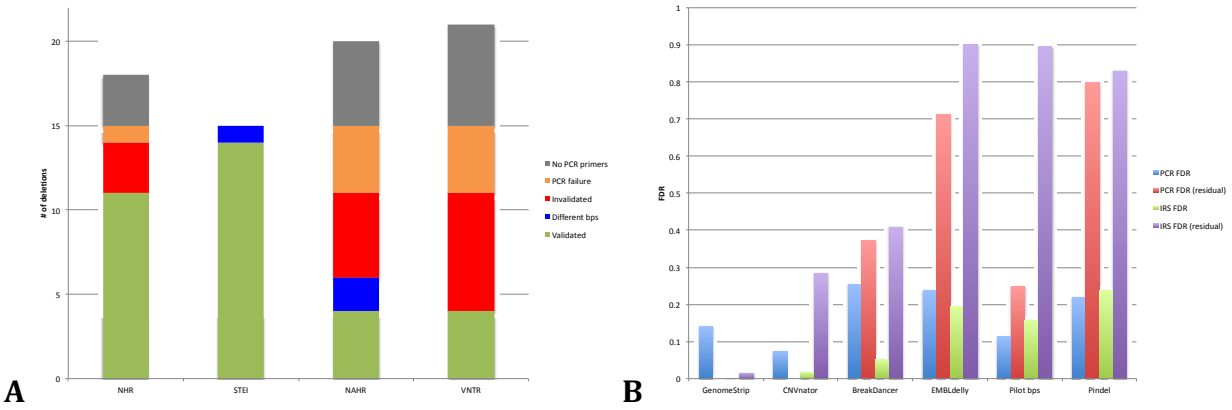

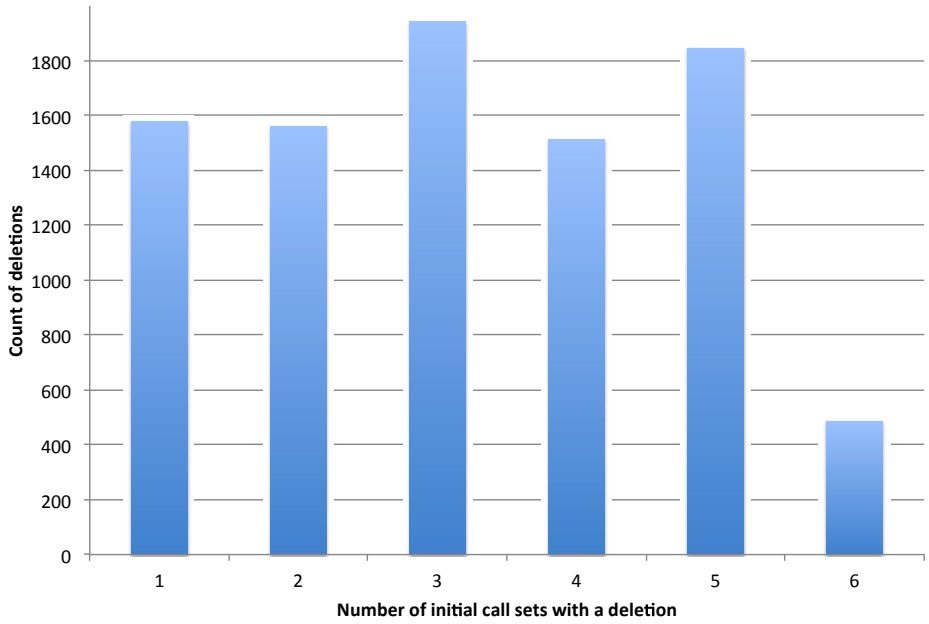

C

Supplementary Figure 11. Validation results before final deletion filtering. A) Breakdown by classification mechanisms. Deletions classified as Variable Number of Tandem Repeats – VNTR do not validate well as their breakpoints are in very repetitive sequences; B) Breakdown by calling method. Methods discovering deletions from split-read analysis (Delly, Pindel, and assembly in the pilot) have overall high FDR and very high residual FDR. C) Breakdown of deletions in the final set by presence in the initial call sets.

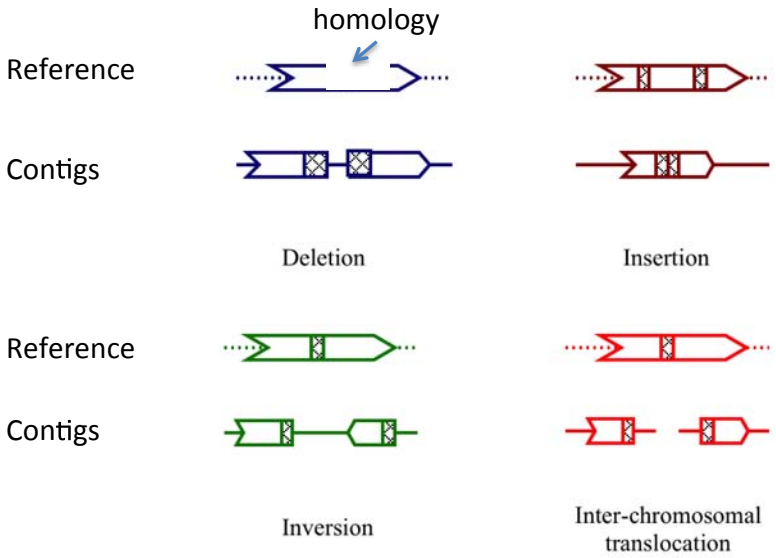

Supplementary Figure 12. Examples of CROSSMATCH alignments to derive breakpoints of structural variations.

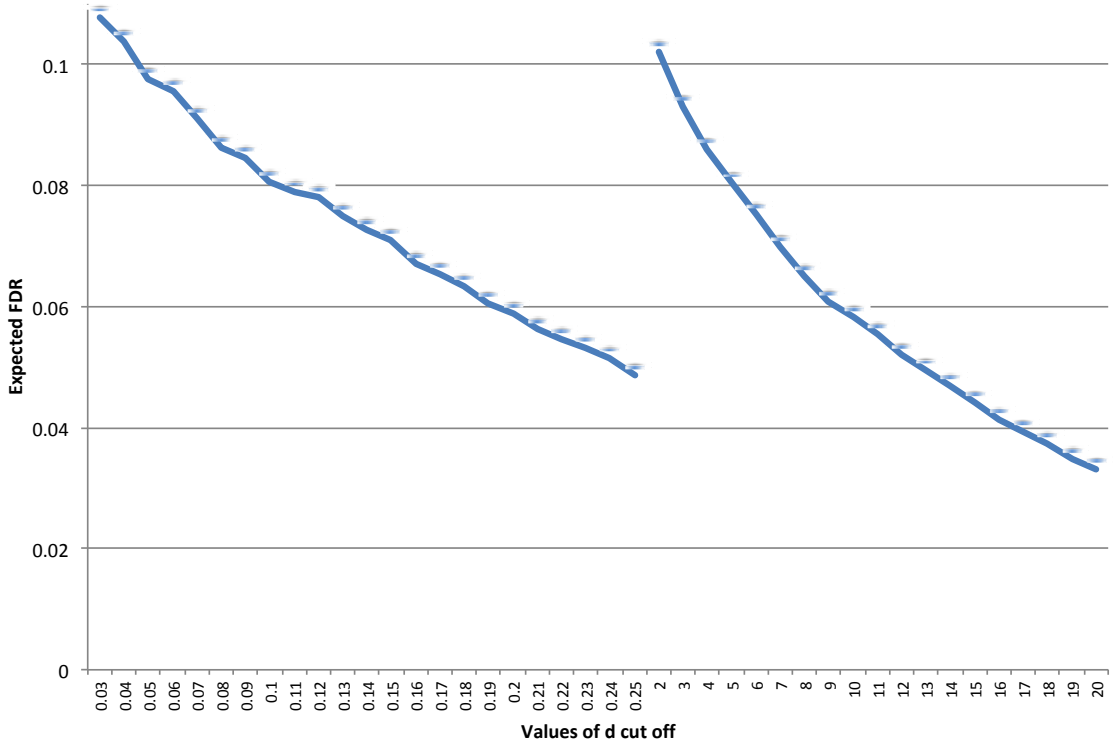

Supplementary Figure 13. *In-silico* FDR for breakpoint support with the values of *d*. When realigning all unmapped reads to the null junction library and varying the value of *d* to compare the number of null junctions passing the filter with the number of real junctions passing the filter. The cutoff *d* is defined as the number/fraction of bases aligned to each flank for deciding, which reads supported breakpoints. Left curve represents the results when *d* is calculated as a fraction of read length. Right curve represents the results when *d* considered in number of bases.

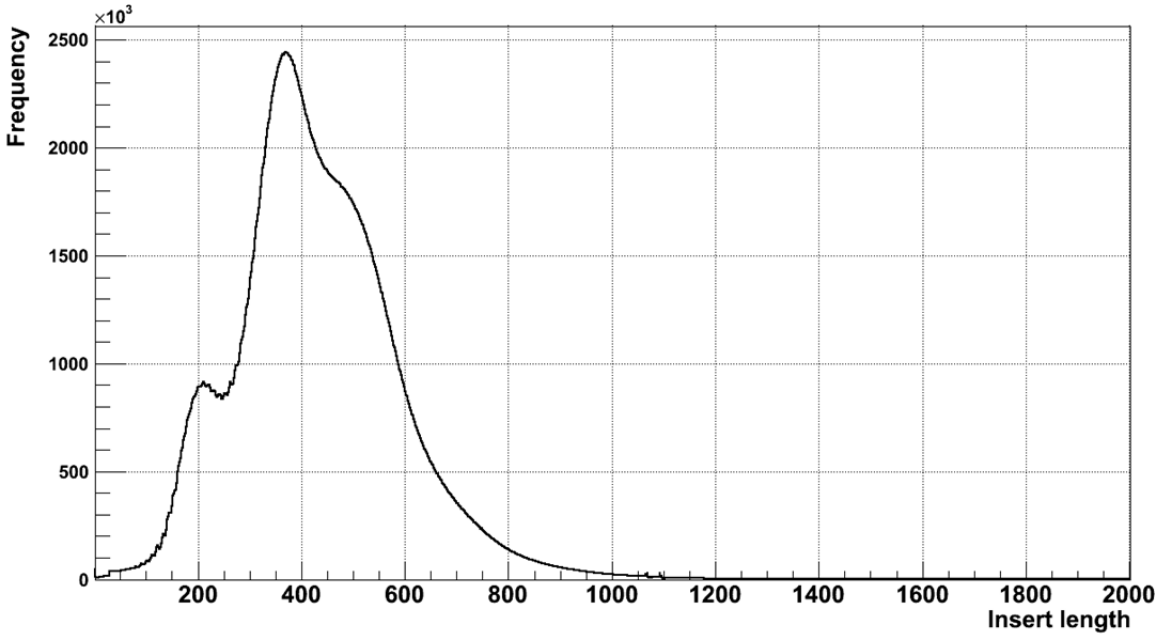

Supplementary Figure 14. Distribution of insert lengths of read pairs in NA12878 Illumina HiSeq 2500 high-coverage data with 250 bp reads. The majority of read pairs significantly overlap at 3'-ends.

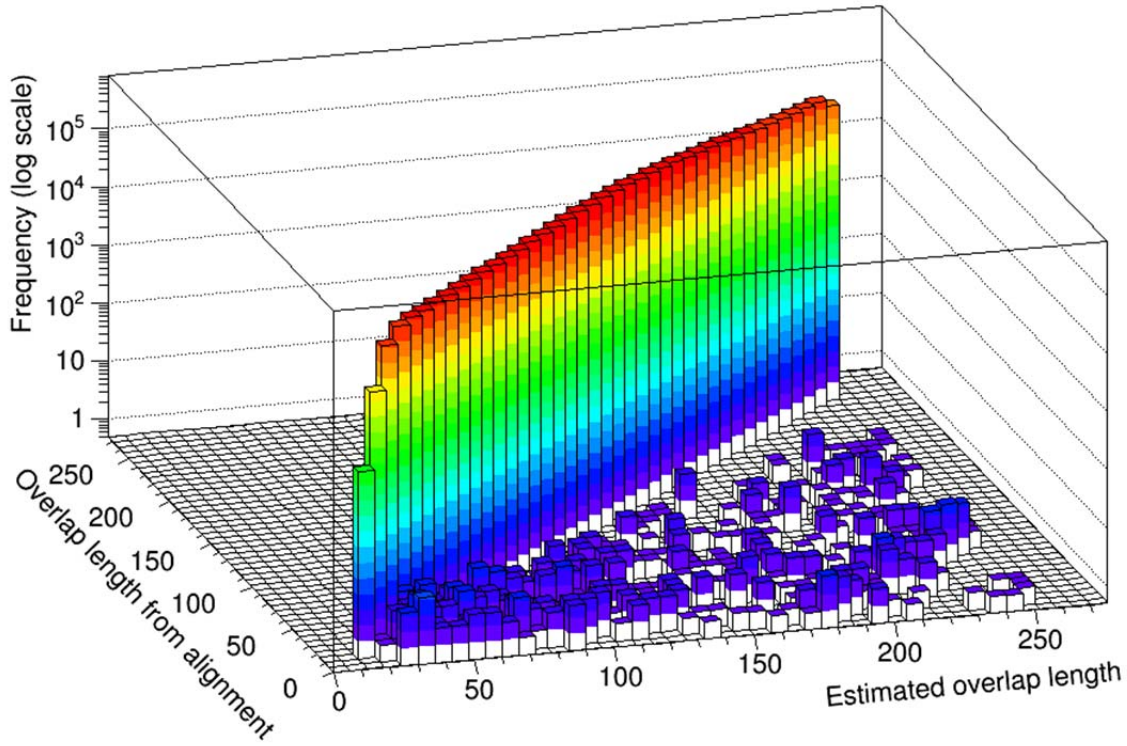

Supplementary Figure 15. Comparison of overlap for reads in the same pair. Two estimates are: i) from sliding reads' 3'-ends against each other; ii) and from independent alignment of reads to the reference genome.

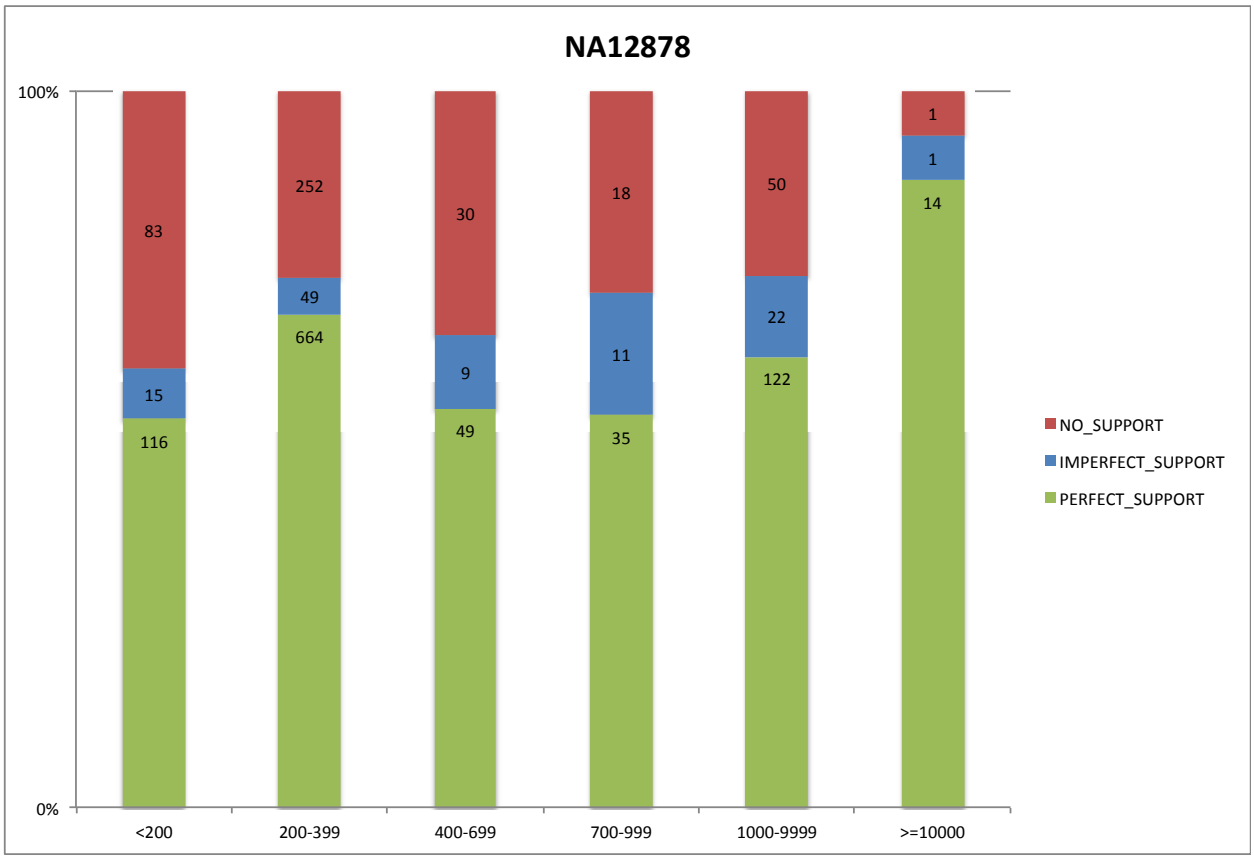

Supplementary Figure 16. Confirmation rate for deletion breakpoints in high coverage individuals. Confirmation across different deletion lengths in NA12878 sample is shown. The confirmation rate decreases with size, reflecting possible genotyping error for small deletions.

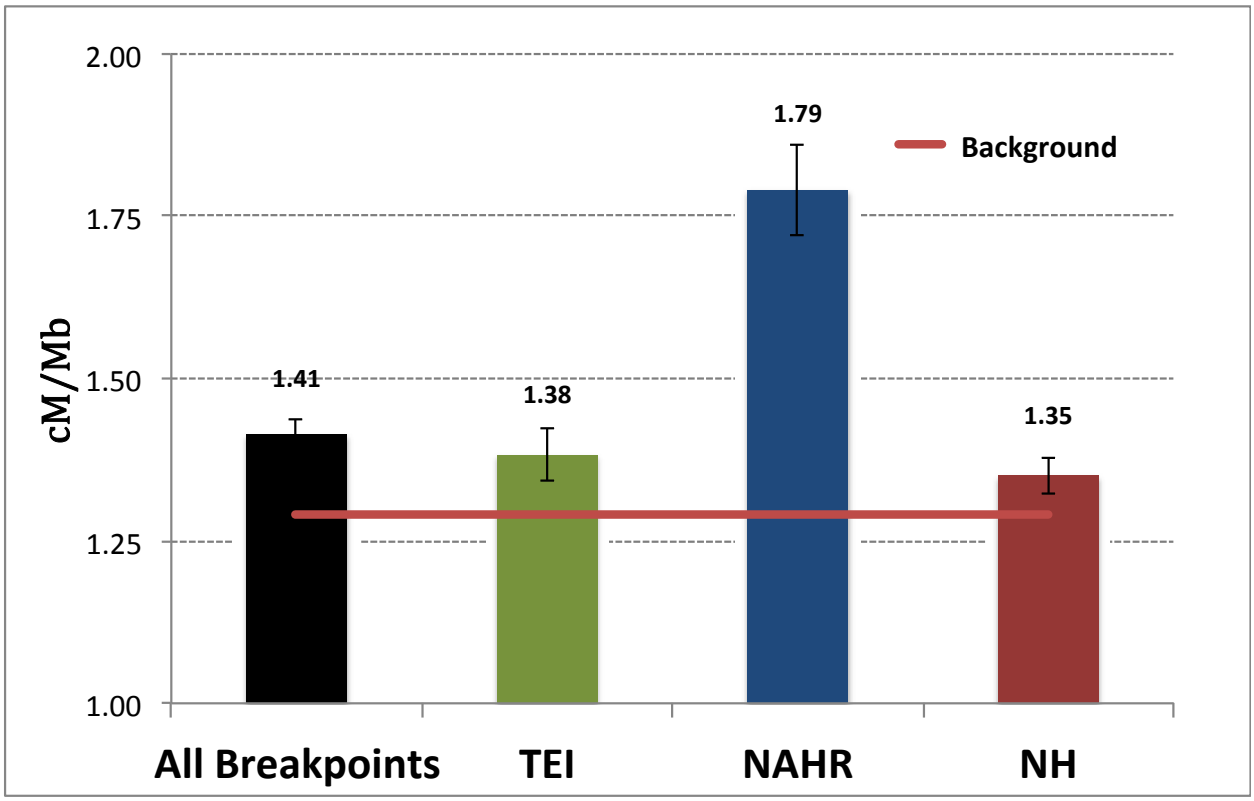

Supplementary Figure 17. Association of breakpoints of different classes with recombination rates across genome. Recombination rates, shown as centimorgans per megabase (Cm/Mb), of different classes of break points from across the genome. Error bars represent 95% confidence interval for each class of breakpoint. The background recombination rate represents the average recombination rate of the genome as a whole.

Supplementary Tables

Supplementary Table 1. Comparison of SV annotations and SV with micro-insertions in different sets.

	# of people	# of variants > 100 bp	NH	NAHR	TEI	VNTR	# with MI	# with MI > 10 bp
Lam et al.[3]	14	1,961	45%	28%	21%	5%	0	0
Kidd et al.[4]	17	1,054	52%	26%	19%	3%	160	82
Conrad et al.[5]	3	324	70-80%*	10-15%*	0%	10-15%*	103	41
Pang et al.[6]*	1	7,330	13%	8%	24%	55%	unknown	0
This study	1,092	8,709	61%	13%	25%	0%	2,391	635

* Including calls that are not at breakpoint resolution, i.e., from **Fig. 3** in Pang et al.[6] and Table 1 in Conrad et al.[5]

Supplementary Table 2. Testing for SNP/indel enrichment around SV breakpoints. Distributions of normalized SNP/indel densities around breakpoints and at large distance were tested by t-test. Regions around breakpoints were defined as a 200 kbps region upstream of the 5'-breakpoints and a 200 kbps region downstream of 3'-breakpoint. Regions at distance were defined between 1 Mbps to 800 kbps upstream of the 5'-breakpoints and between 800 kbps and 1 Mbps downstream of 3'-breakpoint. Regions were divided into bins of 40 kbps in length. Bonferroni correction was applied given that we did 42 tests: 21 for SNPs and 21 for indels.

Breakpoint type	SNP/indel type	Raw p-value	Bonferroni corrected p-value, * -- significant
NH	All	5.80×10^{-7}	**2.44×10^{-5}***
	C>A	2.48×10^{-7}	**1.04×10^{-5}***
	C>G	5.91×10^{-7}	**2.48×10^{-5}***
	C>T	1.51×10^{-6}	**6.35×10^{-5}***
	T>A	1.58×10^{-7}	**6.63×10^{-6}***
	T>C	4.79×10^{-7}	**2.01×10^{-5}***
	T>G	8.12×10^{-9}	**3.41×10^{-7}***
TEI	All	6.48×10^{-4}	**2.72×10^{-2}***
	C>A	1.64×10^{-3}	6.90×10^{-2}
	C>G	8.86×10^{-3}	3.72×10^{-1}
	C>T	2.00×10^{-3}	8.40×10^{-2}
	T>A	1.15×10^{-4}	**4.83×10^{-3}***
	T>C	1.56×10^{-3}	6.55×10^{-2}
	T>G	8.92×10^{-4}	**3.75×10^{-2}***
NAHR	All	6.23×10^{-5}	**2.62×10^{-3}***
	C>A	1.64×10^{-4}	**6.89×10^{-3}***
	C>G	3.74×10^{-1}	1
	C>T	6.82×10^{-6}	**2.86×10^{-4}***
	T>A	8.35×10^{-6}	**3.51×10^{-4}***
	T>C	2.08×10^{-1}	1
	T>G	1.23×10^{-1}	1

Supplementary References

1. 1000 Genomes Project Consortium *et al.* An integrated map of genetic variation from 1,092 human genomes. *Nature* **491,** 56–65 (2012).
2. Bock, C., Walter, J., Paulsen, M. & Lengauer, T. CpG island mapping by epigenome prediction. *PLoS Comput Biol* **3,** e110 (2007).
3. Lam, H. Y. K. *et al.* Nucleotide-resolution analysis of structural variants using BreakSeq and a breakpoint library. *Nat Biotechnol* **28,** 47–55 (2010).
4. Kidd, J. M. *et al.* A human genome structural variation sequencing resource reveals insights into mutational mechanisms. *Cell* **143,** 837–847 (2010).
5. Conrad, D. F. *et al.* Mutation spectrum revealed by breakpoint sequencing of human germline CNVs. *Nat Genet* **42,** 385–391 (2010).
6. Pang, A. W. C., Migita, O., MacDonald, J. R., Feuk, L. & Scherer, S. W. Mechanisms of formation of structural variation in a fully sequenced human genome. *Hum. Mutat.* **34,** 345–354 (2013).